Rock Mech Rock Eng (2015) 48:427–439
DOI 10.1007/s00603-014-0565-1

ORIGINAL PAPER

Water Retention Characteristics and State-Dependent Mechanical and Petro-Physical Properties of a Clay Shale

Katrin M. Wild · Linda P. Wymann · Sebastian Zimmer · Reto Thoeny · Florian Amann

Received: 15 November 2013 / Accepted: 24 February 2014 / Published online: 15 March 2014

Abstract A series of clay shale specimens in equilibrium with various humidity conditions were used to establish the water retention characteristics, the influence of suction on ultrasonic p-wave velocity and rock mechanical properties such as Young's modulus, Poisson's ratio, onset of dilatancy, unconfined compressive strength and Brazilian tensile strength. Opalinus Clay, a clay shale considered as host rock for the disposal of nuclear waste in Switzerland was utilized. The results showed that the p-wave velocity normal to bedding ($v_{p,n}$) dropped sharply upon desaturation until suction approached the air-entry value. The sharp decrease was associated with desiccation cracks solely oriented parallel to bedding. For suction in excess of the air-entry value, $v_{p,n}$ was constant, indicating no further desiccation damage. The suction at the shrinkage limit and at the air-entry point is similar in magnitude. The p-wave velocity parallel to bedding ($v_{p,p}$) remained constant in the entire range of suction investigated in this study. The constant $v_{p,p}$ with increasing suction might be associated with the disproportional decrease in the Poisson's ratio and Young's modulus and its opposing effect on p-wave velocity. An almost linear increase in unconfined compressive strength, Brazilian tensile strength, stress at the onset of dilatancy and Young's modulus with increasing suction was observed up to a suction of 56.6 MPa. For suction larger than 56.6 MPa, relatively constant strength and stiffness was observed. The increase is associated with the net contribution of suction to strength/stiffness, which decreases nonlinearly with decreasing volumetric water content. The rate of increase in tensile strength and unconfined compressive strength with increasing suction is different depending on the rock anisotropy. Compared to the strength values (Brazilian tensile and uniaxial compressive strength) obtained from specimens loaded parallel to bedding, the tensile strength parallel to bedding and the unconfined compressive strength obtained from specimens loaded normal to bedding are considerably more affected by increasing suction or decreasing water content. The reasons for the different rates in strength increase are considered to be related to local variations in suction (i.e., local suction) as a consequence of zones of contrasting pore-size distribution. These variations may influence the effect of suction on strength, especially when the load is applied parallel to bedding and crack growth occurs predominately along bedding layers with comparably low suction.

Keywords Water retention characteristics · Opalinus Clay · Clay shale · Suction · Strength variation · Onset of dilatancy · State-dependent anisotropy

K. M. Wild (✉) · L. P. Wymann · S. Zimmer · R. Thoeny · F. Amann
Institute of Geology, Engineering Geology, Swiss Federal Institute of Technology, Zurich, Sonneggstrasse 5, 8092 Zurich, Switzerland
e-mail: katrin.wild@erdw.ethz.ch

L. P. Wymann
e-mail: lwymann@student.ethz.ch

S. Zimmer
e-mail: zimmers@student.ethz.ch

R. Thoeny
e-mail: reto.thoeny@erdw.ethz.ch

F. Amann
e-mail: florian.amann@erdw.ethz.ch

1 Introduction

Numerous experimental studies revealed that the moisture content of laboratory specimen can have a major influence

on the strength and deformability of soils and rocks (Dyke and Dobereiner 1991; Hsu and Neson 1993; Lashkaripour and Passaris 1995; Wild 2010; Valès et al. 2004; Fredlund et al. 1987; Escario et al. 1989; Rahardjo et al. 1995; Cui and Delage 1996; Feuerharmel et al. 2006; Chae et al. 2010; Nam et al. 2011; Schnellmann et al. 2013). It was consistently shown that the increasing strength or stiffness, along with decreasing moisture content, is associated with capillary forces arising from both the pressure difference between the wetting and the non-wetting fluid at the gas/liquid boundary (capillary suction), and osmotic processes (osmotic suction) in a partly saturated system composed of solids, air and water (Schmitt et al. 1994; Fredlund et al. 1978; Birle 2012). The total suction, further referred to simply as suction, is the sum of capillary and osmotic suction. Surface tension at the boundary between water and air in adjoining voids causes a compressive contact pressure between grains, which increases the shear resistance. This additional resistance has the same effect as if the grains were held together with a cohesive strength component and is often called the *apparent cohesive strength component* (Peterson 1988; Fredlund et al. 1978; Schmitt et al. 1994; Papamichos et al. 1997).

West (1994) analyzed the effect of suction on the uniaxial compressive strength (*UCS*) of various sand- and limestones, and found that for suction between 0 and approximately 10 MPa, the *UCS* of these rock types is little affected. When the suction exceeds approximately 10 MPa, the *UCS* increased markedly. Similar results have been reported by Ramos Da Silva et al. (2008) for low-porosity shales. Schmitt et al. (1994) investigated the dependency of *UCS* on suction for Tournemire shale, Vosges and Fontainebleau sandstone. For Vosges and Fontainebleau sandstone, where the pore space is associated with pore radii larger than 0.1 µm, suction larger than 1 MPa developed when the saturation dropped below approximately 10 %. The increase in suction from 1 to 8–9 MPa (for a decrease in saturation from 10 to 2 %) was accompanied with an increase in *UCS* (e.g., for Vosges Sandstone the *UCS* increased from 25 to 37 MPa.[1]). When the saturation was larger than 10 %, the *UCS* was unaffected. For Tournemire shale, where the pore space is primarily associated with pore radii smaller than 0.1 µm, the water retention characteristics were substantially different, and suction larger than 1 MPa developed already when the saturation dropped slightly below 100 % (Schmitt et al. 1994). The increasing suction in the shale was associated with a continuous increase in *UCS* (i.e., the *UCS* at a saturation of 66.5 % was 19.8 MPa, and at 24.5 % it was 60 MPa). Based on pore-size distribution and water retention characteristics, Schmitt et al. (1994) proposed a saturation threshold for which decreasing saturation becomes significant for the *UCS*. For rock types with predominately micro- and meso-pores, such as Tournemire shale, this threshold is already exceeded by little changes in saturation (from an initially saturated state). These little changes can cause a significant increase in suction accompanied by a measurable increase in the unconfined compressive strength.

The aforementioned studies consistently showed that suction can have a substantial influence on rock mechanical properties, such as the compressive strength and stiffness. This is particularly relevant for rock types with predominately micro-pores, such as mudrocks or clay shales. In such rocks, a small decrease in saturation from an initially saturated state may lead to considerable suction. Thus, the strength and stiffness properties of these partially saturated specimens may not be representative for the in situ properties.

In this study, a series of Brazilian tensile and unconfined compressive strength tests on Opalinus Clay (OPA) specimens were used to establish water retention characteristics and a relationship between suction and rock mechanical properties. The study focuses on the influence of suction on the Young's modulus, Poisson's ratio, the stress threshold at the onset of dilatancy, the uniaxial compressive strength and the tensile strength. The latter was investigated both normal and parallel to bedding, while the other properties were determined parallel to bedding. The influence of increasing suction on the ultrasonic p-wave velocity parallel and perpendicular to the bedding was also investigated.

2 Material Description

For this study, samples from the shaley facies of Opalinus Clay at the Mont Terri research laboratory in Switzerland were utilized. The mass fractions of the predominant mineralogical components of the shaley facies are clay minerals (50–66 %), quartz (10–20 %), carbonates (8–20 %) and feldspar (3–5 %) (Thury and Bossart 1999; Klinkenberg et al. 2009). The mass fraction of clay minerals is composed of 20–30 % 2:1 layer and mixed layer silicates, 7–8 % chlorite and 20–25 % kaolinite (Klinkenberg et al. 2009). Clay platelets are tabular-shaped and lie sub-parallel with the macroscopic bedding, which is made up of siderite concretions and silt and sandstone lenses. The water loss porosity of the shaley facies varies between approximately 13–20 % (Thury and Bossart 1999). The hydraulic conductivity of the shaley facies varies between 10^{-12} m/s parallel to bedding and 10^{-14} m/s normal to bedding (Thury and Bossart 1999).

[1] In this paper, the geomechanics convention is used, with tension denoted as negative number, and compression denoted as positive number

Houben et al. (2013) analyzed the pore-size distribution of the shaley facies using various methods. They suggest that the majority of equivalent pore radii are in a range between approximately 0.003–0.1 μm. They also found that the representative element area (REA) for the mineralogical composition and pore-size distribution is 100×100 μm^2 (i.e., for areas larger than the REA, fluctuation in mineralogical composition and porosity are negligible).

3 Sampling and Testing Methods

3.1 Sampling, Specimen Handling and Specimen Preparation

Opalinus Clay samples were taken from 61-mm-diameter cores obtained from a 38-m-long borehole (BFE-A3) in the shaley facies at the Mont Terri Underground Rock Laboratory. Double-tube core barrels with compressed air cooling were utilized, and specimens were hermetically sealed in vacuum-evacuated foil immediately after core extraction.

All specimens were cut under dry conditions at the Institute of Structural Engineering at the Swiss Federal Institute of Technology in Zurich, using a rigid prismatic specimen-holder and an electronically controlled diamond-saw (WELL, Model 6234). The constant band rotating speed, the constant feed rate and the thin metal string (0.3 mm) populated with diamonds allows for vibration-less cutting. Specimens for Brazilian tensile strength testing were cut to a diameter–height ratio of 2:1, those for the uniaxial compressive strength tests to 1:2. After cutting, the end-faces were polished. Parallelism of the end-faces met the requirements of the ISRM suggested methods (ISRM 1978, 1979a). The environmental exposure time of the specimens was minimized through a rigorous preparation procedure and immediate sealing of the specimens between subsequent preparation steps.

3.2 Water Content and Degree of Saturation

The mass fraction of water (ω) and saturation were determined according to ISRM suggested methods (ISRM 1979b). The volumetric water content (θ) was calculated using the following equation

$$\theta = \omega \cdot \rho_d \tag{1}$$

where ρ_d is the dry density which is related to the bulk density (ρ_{bulk}) and the water content (ω) by the following relationship

$$\rho_d = \frac{\rho_{bulk}}{1 + \omega} \tag{2}$$

Table 1 Saline solutions and the corresponding theoretical and achieved relative humidity. The suction values correspond to the achieved relative humidity

Salt solution	Relative humidity		Suction (MPa)
	Theoretical (%)	Achieved (%)	
K_2SO_4	>97	97/99	4.1/1.4
KCl	84–85	85	22.0
NaCl	75	75	39.0
$NaNO_2$	66	66	56.3
$Ca(NO_3)_2$*$(4H_2O)$	51–54	52/53	88.6/86.0
K_2CO_3	43	43	114.3
$CaCl_2$	29–31	31/38	158.6/131.0
LiCl	15	19	224.9

The water loss porosity (ϕ) was derived from the dry density (ρ_d) and grain density (ρ_s) using

$$\phi = 1 - \frac{\rho_d}{\rho_s} \tag{3}$$

The grain density is given as 2.7 ± 0.2 g cm^{-3} (Bock 2008). The degree of saturation (S_w) was calculated using

$$S_w = \frac{\omega \rho_d}{\phi \rho_w} \tag{4}$$

where ρ_w is the density of water.

3.3 Water Retention Curve

Water retention characteristics were established from specimens exposed to various levels of humidity in desiccators under stress free conditions. Constant predefined relative humidity was achieved and maintained by utilizing supersaturated salt solutions (Table 1). While exposing the specimens to these different environments, the air temperature in the laboratory was held constant at 21 ± 0.5 °C, and the relative humidity in the desiccators was monitored. The correspondent suction pressure was calculated according to Kelvin's relationship:

$$\psi = -\frac{R \cdot T}{V_{w0} \cdot \omega_w} \ln\left(\frac{p}{p_0}\right) \tag{5}$$

where ψ is the suction in Pa, R the ideal gas constant in J/mol/K, T the absolute temperature in Kelvin, V_{w0} the specific volume of water (i.e., the inverse of the water density) in m^3/kg, ω_w the molecular mass of water vapor, p the vapor pressure of water in the system in MPa and p_0 the vapor pressure of pure water in MPa. The term p/p_0 is the relative humidity as given by the experimental setup. The suction values utilized in this study are given in Table 1 and range from 1.4 to 224.9 MPa.

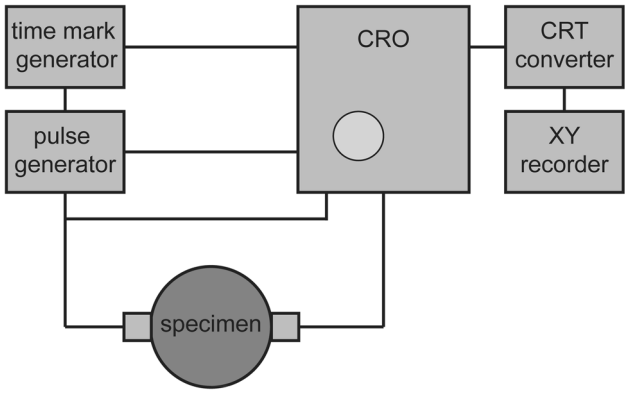

Fig. 1 Components of the high-frequency ultrasonic pulse measurement

Specimens were dried or saturated to constant weight, and the degree of saturation at each applied suction was determined as outlined above. The experimentally observed relationship between saturation and suction was fitted to the Van Genuchten equation (Eq. (6), with fitting parameters P_0 and β, according to Van Genuchten 1980) to establish the water retention curves for both, drying and wetting path.

$$S_w = \left[1 + \left(\frac{\psi}{P_0}\right)^{1/(1-\beta)}\right]^{-\beta} \quad (6)$$

3.4 Ultrasonic P-wave Velocity Measurements

P-wave velocity was measured utilizing high-frequency ultrasonic pulse technique. A *proceq* ultrasonic pulse device was used, which is composed of an impulse generator, transducer (transmitter and receiver), time mark generator and a cathode ray oscilloscope (Fig. 1). A pulse width of 1–10 s and a frequency of 54 kHz were utilized. The repetition frequency mounts up to 10–10^3 repetitions per second. The velocity was derived by dividing the measured travel time by the specimen's length or diameter, respectively. Before each measurement, the sensor array was calibrated with a calibration rod. Ultrasonic p-wave velocity parallel ($v_{p,p}$) and perpendicular ($v_{p,n}$) to the bedding plane orientation were obtained from specimens in equilibrium with the applied suction (Fig. 2). Additionally, one specimen was dried at ambient conditions (i.e., 37 % relative humidity and 22 °C on average) in the laboratory with simultaneous monitoring (in intervals of 15 min) of the weight loss and the p-wave velocity normal to bedding.

3.5 Mechanical Testing Procedure

Brazilian and uniaxial compression tests were performed at the rock mechanical laboratory at the Swiss Federal Institute of Technology in Zurich (Chair of Engineering Geology). A modified 2,000 kN *Walter and Bai* servo-hydraulic rock testing device with digital feedback control was utilized.

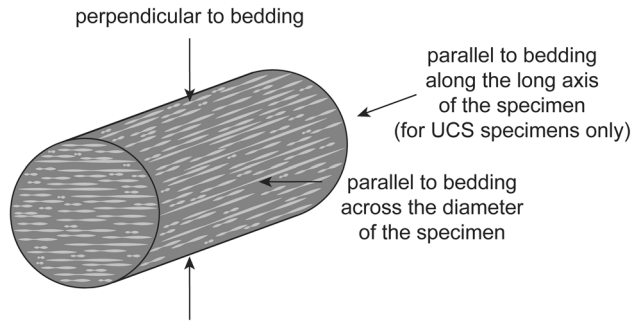

Fig. 2 P-wave velocity measurements with respect to bedding

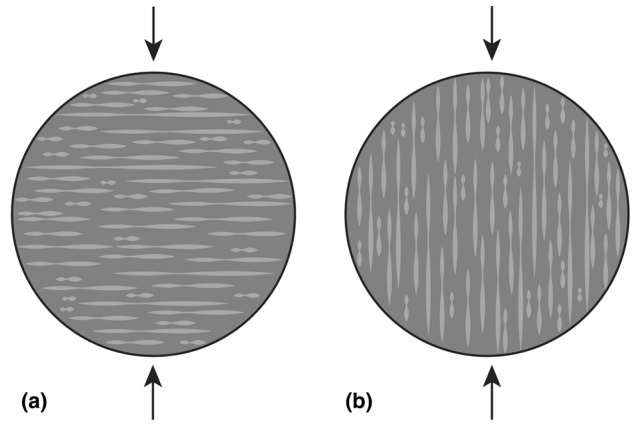

Fig. 3 Loading configurations for Brazilian tests with respect to bedding: load is applied **a** parallel or **b** perpendicular. For configuration **a** the Brazilian tensile strength parallel ($\sigma_{t,p}$) to bedding was obtained, for **b** normal to bedding ($\sigma_{t,n}$)

Brazilian tests were performed with a constant loading rate of 0.1 kN/min. The load was applied parallel or normal to bedding (Fig. 3). For the unconfined compressive strength tests, load was applied in direction parallel to bedding in such a way as to maintain a constant circumferential displacement rate. The selected rate for the tests was 0.04 to 0.08 mm/min for specimens conditioned at high relative humidity (i.e., 75, 95 and 99 %), and 0.01 mm/min for specimens exposed to lower relative humidity. Since the loading rates were high and the hydraulic conductivity of this clay shale is low, the tests are considered undrained. Axial and circumferential strain gages were mounted onto the specimen at half of the specimen height to eliminate the influence of end effects on the strain measurements (Fig. 4). Two axial strain gages (Type BD 25/50, DD1), each with a base-length of 50 mm, were firmly attached on opposite sides of the specimens.

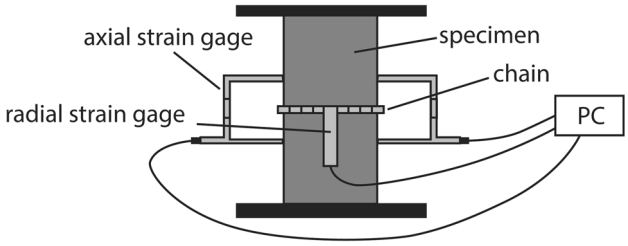

Fig. 4 Monitoring setup for unconfined compression tests

The radial strain (ε_{radial}) was calculated from the displacement measured by a single gage (Type 3544-150M-120m-ST), which was attached to a chain wrapped tightly around the specimen (Fig. 4).

3.6 Determination of the Onset of Dilatancy and Elastic Parameters

For unconfined compression tests, two strain-based methods were utilized to determine the onset of dilatancy (*CI*). The two different strain-based approaches are illustrated in Fig. 5a, b:

1. Brace et al. (1966) suggested that the onset of dilation can be established by examining when the axial stress–volumetric strain curve deviates from its linear portion at low axial stress (Fig. 5a). Volumetric strain (ε_{vol}) was calculated from the sum of the arithmetic mean of the two axial strains (ε_{axial}) and twice the radial strain (ε_{radial}):

$$\varepsilon_{vol} = \varepsilon_{axial} + 2\varepsilon_{radial} \quad (7)$$

2. Lajtai (1974) applied the same principle as Brace et al. (1966) to the axial stress–radial strain curve. The onset of dilatancy is taken at the point where the radial strain curve deviates from linearity (Fig. 5b).

Both, Young's modulus (E) and Poisson's ratio (υ) were obtained from the linear part of the stress–axial strain curve at low axial stresses (i.e., axial stress < *CI*).

4 Results

4.1 Water Retention Characteristics

Figure 6 shows the relationship between water content and suction obtained from specimens with water loss porosities between 15 and 19 %. The relationship between saturation and suction for the same specimens is shown in Fig. 7.

Data points for desorption (drying) represent several individual specimens conditioned in desiccators with relative humidity between 19 and 85 %. The scatter in the degree of saturation for the same applied suction is most probably associated with the natural variability in pore-size distribution. The adsorption path (wetting) was obtained from specimens that were consecutively saturated in six desiccators with relative humidity ranging from 38 to 85 %. Specimens which were placed in desiccators at 97 and 99 % relative humidity, immediately after dismantling, showed a slight increase in water content in the order of 1 %, suggesting that the specimens were not saturated. These specimens are further considered to be representative for the wetting path.

Drying and wetting path are both nonlinear (Fig. 6). Data further shows that the water content and saturation degree are reversible, following a hysteresis loop. The hysteresis between wetting and drying path becomes clearer when saturation is plotted against suction as shown in Fig. 7. The reversibility of water content and saturation suggests that air entrapment in the rock is negligible.

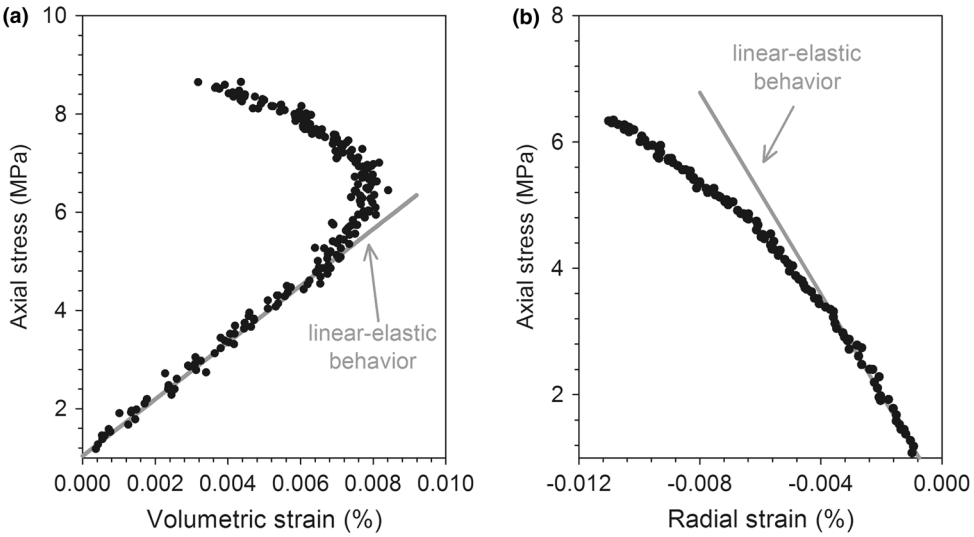

Fig. 5 Methodology for determining the onset of dilatancy in unconfined compression tests by examining **a** the volumetric strain response according to Brace et al. (1966) and **b** the radial strain response according to Lajtai (1974)

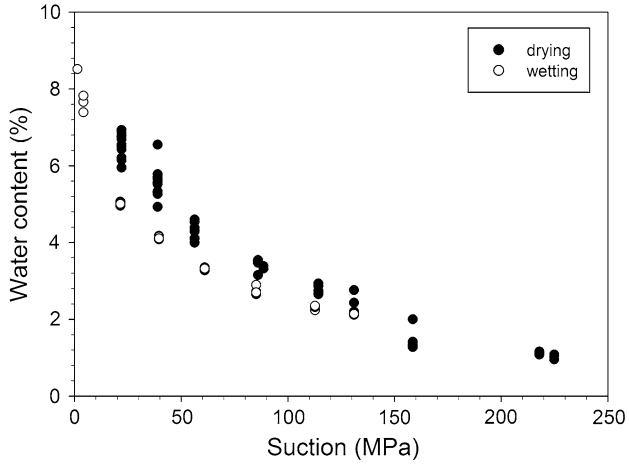

Fig. 6 Relationship between water content and suction

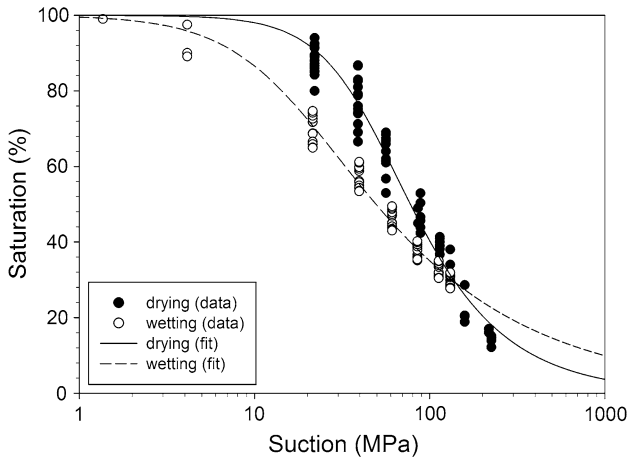

Fig. 7 Relationship between saturation and suction. The data points were fitted to the Van Genuchten equation (Van Genuchten 1980)

Experimental data in Fig. 7 were fitted to the Van Genuchten equation (see Eq. (6), Van Genuchten 1980). The corresponding fitting parameters are given in Table 2. The drying path was used to derive an estimate of the air-entry suction (i.e., the suction where air theoretically enters the larger pores of the specimen). The air-entry value was determined by extending the tangent of the central part of the Van Genuchten fit to its intersection with the saturation axis (i.e., where saturation equals 1.0, Fig. 8). A value of 22 MPa was found. Data and water retention curves obtained in this study are in agreement with the water retention characteristics obtained from the shaley facies of OPA by Ferrari and Laloui (2013) using psychrometer measurements on specimens with different water contents (Fig. 9).

4.2 Variations in Ultrasonic P-wave Velocity

Figure 10 shows the mean values and standard deviations of ultrasonic p-wave velocities obtained from cylindrical

Table 2 Fitting parameters for the water retention curves. The deviations given in parentheses correspond to the 95 % confidence interval

	Drying path	Wetting path
P_0	47.4 (±3.0)	15.7 (±1.45)
β	0.52 (±0.02)	0.36 (±0.01)

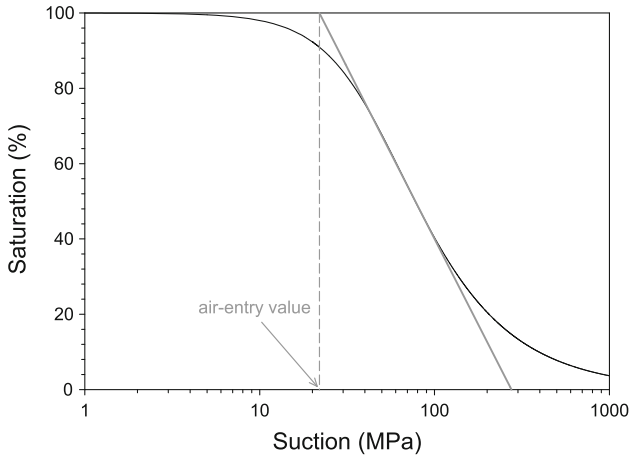

Fig. 8 Determination of the air-entry point. The air-entry suction was found to be 22 MPa

specimens in equilibrium with the applied suction (Table 1). Also shown in Fig. 10 are mean p-wave velocities measured immediately after core dismantling, and p-wave velocities reported by Amann et al. (2011, 2012) obtained immediately after core dismantling. Suction values of the latter specimens were estimated using the relationship between water content and suction as shown in Fig. 6 and are found to be approximately 12 and 7 MPa, respectively.

The p-wave velocities measured parallel to bedding ($v_{p,p}$) were nearly constant at a value of 3,000 m/s for the entire range of suction tested and remained constant for the drying and wetting path. This is in contrast to the p-wave velocity normal to bedding ($v_{p,n}$). A slight increase in suction from its initial stage (i.e., after core dismantling) was associated with a substantial drop in $v_{p,n}$ from 2,250 m/s at 12 MPa suction to 1,000 m/s at 22 MPa suction. This sharp drop in $v_{p,n}$ was also observed within 0–3 h of drying under ambient conditions and remained constant at 1,000 m/s for an elapsed time of >26 h (Fig. 11). For suction larger than 22 MPa, $v_{p,n}$ was nearly constant at 1,000 m/s, for both, wetting and drying path (Fig. 10). For the wetting path, $v_{p,n}$ remained at around 1,000 m/s, even for applied suctions smaller than 22 MPa. This indicates that the major drop in $v_{p,n}$ is irreversible.

4.3 Variations in Elastic Properties

Figures 12 and 13 show variations in Young's modulus and Poisson's ratio, respectively, related to changes in suction.

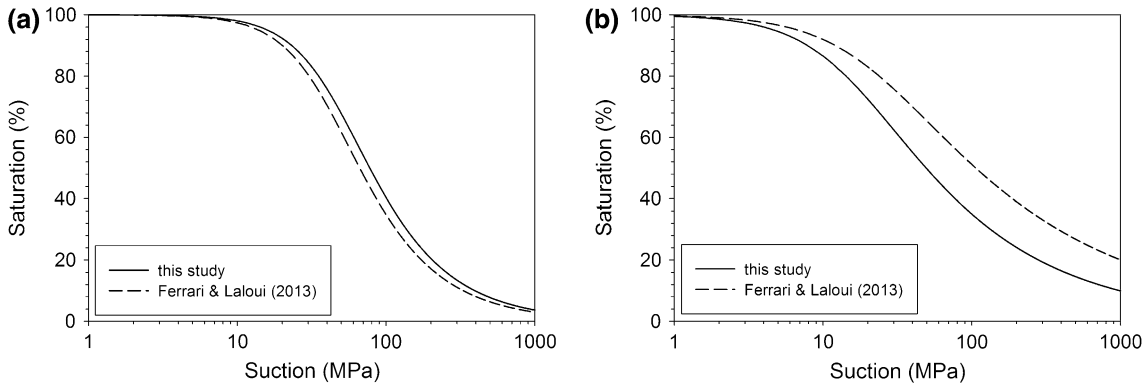

Fig. 9 Comparison of water retention curves obtained in this study with curves obtained by Ferrari and Laloui (2013): **a** drying path, **b** wetting path

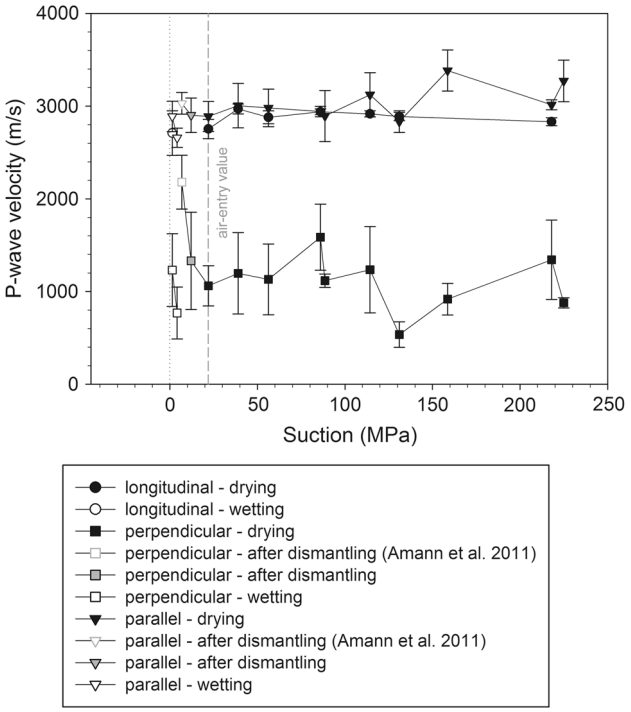

Fig. 10 Relationship between p-wave velocity normal and parallel to bedding and suction

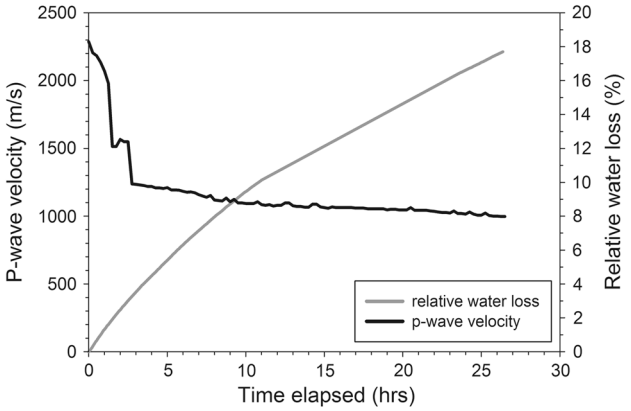

Fig. 11 Evolution of the p-wave velocity (measured normal to bedding) and relative water loss with time obtained from a specimen dried under ambient conditions (i.e., 22 °C and 37 % relative humidity on average)

Both, the mean values and the data range (i.e., the minimum and maximum measured values) are shown for the corresponding applied suction (see also Table 4). For specimens that were tested immediately after core dismantling and specimen preparation, the equivalent suction was estimated to be approximately 13 MPa, using the relationship between water content and suction (Fig. 6).

The Young's modulus increases almost linearly from 6.7 GPa after core dismantling to 23.3 GPa for a suction of 56.6 MPa. Between 56.6 and 224.9 MPa suction, E does not tend to further increase, even though the scatter is high in this range of suction. The Poisson's ratio exhibits an opposing, but similar trend as E. The Poisson's ratio decreases from approximately 0.20 after core dismantling to 0.11 at a suction of 56.6 MPa. For suction larger than 56.6 MPa, the Poisson's ratio varies around a mean value of 0.11.

4.4 Variations in Strength

4.4.1 Tensile Strength

Figure 14 shows the mean, minimum and maximum Brazilian tensile strength (σ_t) parallel ($\sigma_{t,p}$) and normal ($\sigma_{t,n}$) to bedding with increasing suction (see also Table 3). It can be seen that $\sigma_{t,p}$ is generally higher than $\sigma_{t,n}$, reflecting the transversal isotropy of Opalinus Clay. For the lowest suction applied in this study (i.e., 1.4 MPa), the anisotropy ratio ($\sigma_{t,p}/\sigma_{t,n}$) is approximately two. With increasing suction, the anisotropy ratio increases, indicating dissimilar increase in $\sigma_{t,p}$ and $\sigma_{t,n}$. Even though the rate of increase with increasing suction is dissimilar, both, $\sigma_{t,p}$ and $\sigma_{t,n}$

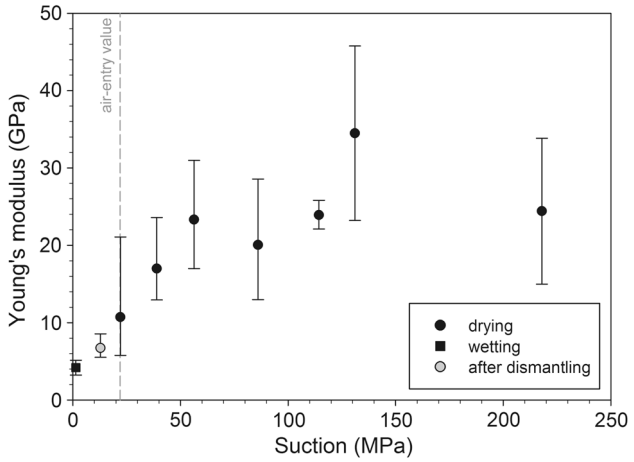

Fig. 12 Relationship between the Young's modulus and suction. Mean value and data range for each applied suction are given

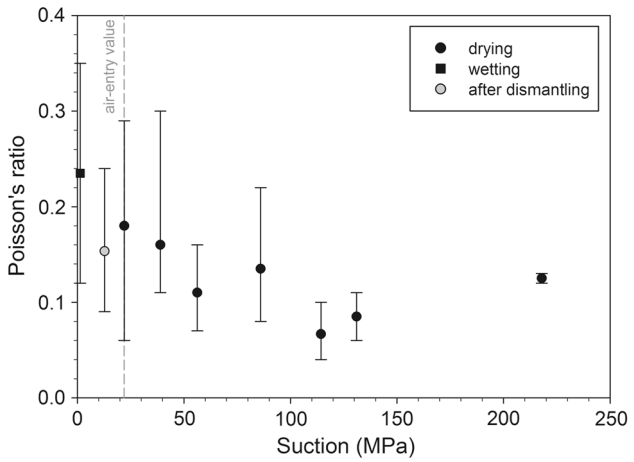

Fig. 13 Relationship between the Poisson's ratio and suction. Mean value and data range for each applied suction are given

exhibit an almost linearly increase up to a suction of 56.6 MPa. The maximum measured σ_t was −1.5 MPa for $\sigma_{t,n}$, and −3 MPa for $\sigma_{t,p}$ (i.e., ~3 times the σ_t at a suction of 1.4 MPa, Fig. 14). For suction larger than 56.6 MPa, $\sigma_{t,n}$ did not tend to increase and varied around a mean value of approximately −1.5 MPa. The $\sigma_{t,p}$, however, dropped in the range of 56.6 to 150 MPa suction to a value of approximately −2 MPa.

4.4.2 Onset of Dilatancy

Figure 15 shows the mean axial stress and axial stress range at the onset of dilatancy, with increasing suction (see also Table 4) obtained from the volumetric and radial strain response. For capillary suction smaller than 56.6 MPa, *CI* increases almost linearly with increasing suction. Beyond 56.6 MPa suction, *CI* was almost constant except for the results obtained from specimens at 224.9 MPa suction,

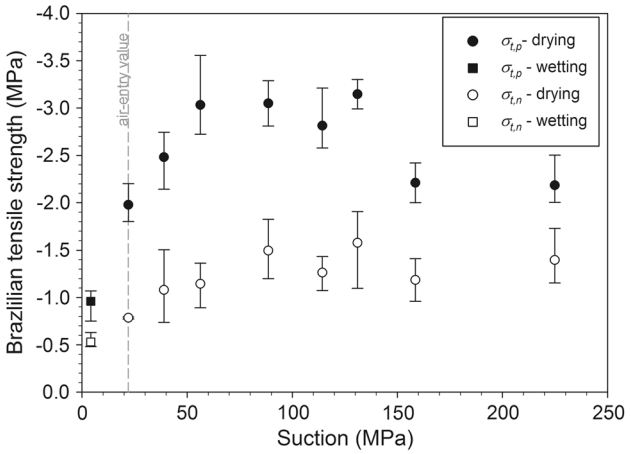

Fig. 14 Relationship between the Brazilian tensile strength (normal and parallel to bedding (i.e., $\sigma_{t,n}$ and $\sigma_{t,p}$)) and suction. Mean value and data range for each applied suction are given

which showed a large variability. The increase in *CI* with increasing suction (in this study, up to an applied suction of 56.6 MPa) is in agreement with results obtained by Dyke and Dobereiner (1991) on sandstone.

CI-values obtained from specimens with an applied suction of 1.4 MPa were 2 MPa on average. The stress at the onset of dilation obtained in this study is consistent with results reported by Amann et al. (2011, 2012), which found an average *CI*-value of 2 MPa for OPA specimens loaded normal to bedding. This suggests that *CI* is equal for both loading directions. *CI* is typically considered as a material property that is stress path independent. However, results obtained in this study show that *CI* is a state property and varies substantially with varying suction.

4.4.3 Uniaxial Compressive Strength

Figure 16 shows the relationship between *UCS* (mean, minimum and maximum for each applied suction) with increasing suction (see also Table 4). Three specimens were tested directly after core dismantling and specimen preparation, and the corresponding suction was estimated from the relationship between water content and suction (Fig. 6) and was 13 MPa on average.

Data show that the *UCS* increases almost linearly between 13 and 56.6 MPa suction. Specimens saturated in desiccators with relative humidity of 99 % (i.e., 1.4 MPa suction) revealed a considerably lower *UCS*. For suction larger than 56.6 MPa, the *UCS* increases nonlinearly, and above a suction of 86 MPa no significant change in *UCS* can be identified.

The low mean *UCS* at 1.4 MPa suction is most probably associated with the conditioning of these specimens at a relative humidity of 99 %, which was difficult to maintain. Short-term humidity cycles (i.e., relative humidity

Table 3 Results of Brazilian tensile strength tests

Specimen number	Suction (MPa)	$\sigma_{t,p}$ (MPa)	Specimen number	Suction (MPa)	$\sigma_{t,n}$ (MPa)
BTS12a	4.1	−0.8	BTS12b	4.1	−0.6
BTS12c	4.1	−1.1	BTS17a	4.1	−0.5
BTS17b	4.1	−1.1	BTS22a	4.1	−0.5
BTS15a	22.0	−2.0	BTS7a	22.0	−0.8
BTS15e	22.0	−2.2	BTS15b	22.0	−0.8
BTS15f	22.0	−1.8	BTS29f	22.0	−0.8
BTS15g	22.0	−1.9	BTS29a	39.0	−1.0
BTS10a	39.0	−2.7	BTS29b	39.0	−0.7
BTS13a	39.0	−2.1	BTS29c	39.0	−1.1
BTS13b	39.0	−2.3	BTS29d	39.0	−1.5
BTS13c	39.0	−2.6	BTS21b	56.3	−0.9
BTS22c	39.0	−2.7	BTS30a	56.3	−1.4
BTS11a	56.3	−3.2	BTS30b	56.3	−1.2
BTS11b	56.3	−2.8	BTS30c	56.3	−1.2
BTS21a	56.3	−2.7	BTS16a	88.6	−1.5
BTS21c	56.3	−2.9	BTS16b	88.6	−1.8
BTS22b	56.3	−3.6	BTS16d	88.6	−1.2
BTS16c	88.6	−3.3	BTS23c	114.3	−1.4
BTS16f	88.6	−2.8	BTS23d	114.3	−1.1
BTS23a	114.3	−2.6	BTS23e	114.3	−1.3
BTS23b	114.3	−3.2	BTS26d	158.6	−1.4
BTS23f	114.3	−2.7	BTS26e	158.6	−1.0
BTS25b	158.6	−2.4	BTS27c	224.9	−1.7
BTS26b	158.6	−2.0	BTS27e	224.9	−1.2
BTS27a	224.9	−2.0	BTS28b	224.9	−1.3
BTS27b	224.9	−2.5	BTS31c	131.0	−1.9
BTS27d	224.9	−2.0	BTS31m	131.0	−1.1
BTS31k	131.0	−3.0	BTS31q	131.0	−1.7
BTS31n	131.0	−3.3			

$\sigma_{t,p}$ Brazilian tensile strength parallel to bedding, $\sigma_{t,n}$ Brazilian tensile strength normal to bedding

variations between 96 and 99 %) were observed. As a consequence, a stable equilibrium could not be reached, and saturation of the specimens exceeded 100 %. Hence, *UCS*-values obtained from these specimens are not considered representative for 1.4 MPa suction. A back-extrapolation of a linear regression through representative data points between 13 and 56.6 MPa suction suggests a *UCS* of approximately 9 MPa for fully saturated specimens.

5 Discussion

5.1 Variations in P-wave Velocity

Figures 6 and 7 suggest that the suction in the specimens is reversible following a hysteresis loop. The p-wave velocity

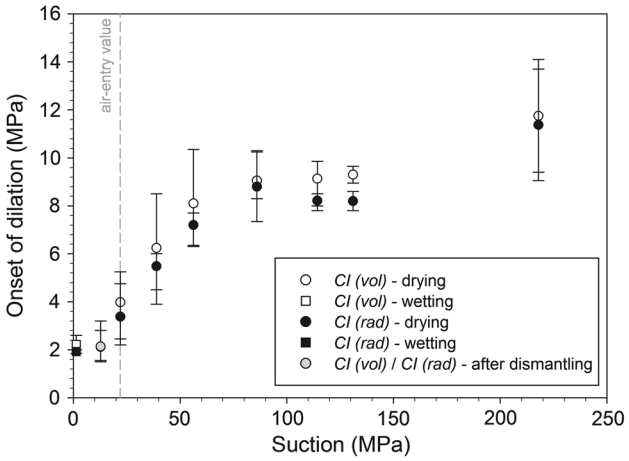

Fig. 15 Relationship between onset of dilation (*CI*) and suction. Mean value and data range for each applied suction are given

normal to bedding is, however, irreversible, suggesting an irreversible alteration of bulk material properties, rather than a direct influence of suction. For the drying path, a sharp decrease in $v_{p,n}$ from 2,250 m/s to 1,000 m/s between 0 and 20 MPa suction was observed. For suction between 20 and 220 MPa, $v_{p,n}$ was almost constant at a value of 1,000 m/s. The sharp decrease in $v_{p,n}$ occurred between 0 and 20 MPa suction and was irreversible for the wetting path. Seismic velocities measured parallel to bedding in the same range of suction were constant at approximately 3,000 m/s.

Peron et al. (2009) found from desiccation experiments on saturated fine-grained soils that upon drying, the void ratio decreases sharply at relatively low suction, accompanied by an increase in deformation rate and desiccation damage. With further increase in suction, both, void ratio and deformation were almost constant. The suction at which the deformation rate sharply decreases is called the shrinkage limit. Peron et al. (2009) showed experimentally that the shrinkage limit and air-entry value are similar in magnitudes, suggesting that the majority of desiccation damage is associated with the early stage of desaturation where the suction increases from 0 to approximately the air-entry value. Desiccation cracking typically occurs when drying shrinkage is constraint, and/or tensile stresses in excess of the tensile strength are generated (Corte and Higashi 1960; Peron et al. 2009). The findings of Peron et al. (2009) are consistent with the findings for $v_{p,n}$ in this study, which decreased sharply between 0 and 22 MPa. In this stage of desaturation formation of desiccation, macro-cracks were observed for all test specimens. For suction larger than 22 MPa, $v_{p,n}$ was almost constant at 1,000 m/s, indicating no further increase in desiccation damage. The transition between the sharp decrease in $v_{p,n}$ and an almost constant $v_{p,n}$ is consistent with the air-entry suction that was found to be 22 MPa.

Table 4 Results from unconfined compressive strength tests

Specimen number	Suction (MPa)	*E* (GPa)	*v*	*UCS* (MPa)	*CI* (*vol*) (MPa)	*CI* (*rad*) (MPa)
5	39.0	23.6	0.30	11.8	4.5	3.9
6	86.0	28.6	0.22	17.2	8.3	7.4
7	56.3	31.0	0.16	14.3	6.4	6.3
8	39.0	16.9	0.14	15.0	6.0	5.9
9	114.3	23.8	0.04	15.3	9.9	8.5
10	22.0	21.0	0.29	11.3	5.3	4.8
11	114.3	25.8	0.06	17.2	7.8	8.0
12	39.0	14.4	0.11	12.9	5.9	5.6
13	56.3	21.9	0.10	13.5	7.6	7.6
14	114.3	22.1	0.10	17.1	9.8	8.2
15	86.0	21.0	0.10	15.7	10.3	8.8
16	56.3	17.0	0.07	15.6	10.4	7.7
17	39.0	17.2	0.13	12.7	8.5	6.0
18	22.0	7.5	0.13	11.5	4.8	3.7
20	56.3	–	–	14.2	–	–
21	217.9	–	–	19.1	–	–
22	22.0	–	–	11.1	–	–
24	86.0	17.7	0.08	16.0	–	10.3
25	217.9	33.8	0.12	22.1	14.1	13.7
26	131.0	23.2	0.06	19.1	9.7	7.8
28	39.0	12.9	0.12	15.6	6.4	6.0
31	131.0	45.8	0.11	13.5	9.0	8.6
32	217.9	15.0	0.13	14.0	9.4	9.1
2	22.0	5.8	0.06	7.8	3.5	2.9
4	22.0	8.6	0.24	6.3	2.5	2.2
34	86.0	13.0	0.14	13.1	8.6	8.8
1	1.4	-	–	2.4	–	–
3	1.4	–	–	1.3	–	–
19	1.4	–	–	3.5	–	–
23	1.4	5.1	0.12	4.6	2.6	2.0
33	1.4	3.2	0.35	3.4	1.9	1.9
UCS 01	12.8	6.1	0.13	9.9	1.6	1.5
UCS 02	12.8	5.5	0.09	12.4	2.0	1.7
27	12.8	8.6	0.24	13.2	2.8	3.2

E Young's modulus, υ Poisson's ratio, *UCS* unconfined compressive strength, *CI (vol)* onset of dilatancy determined according to Brace et al. (1966), *CI (rad)* onset of dilatancy determined according to Lajtai (1974)

The material tested in this study is anisotropic in strength, with a tensile strength parallel to bedding, which is approximately twice the tensile strength normal to bedding (i.e., tensile strength after dismantling of the specimens, Fig. 14). The anisotropy in tensile strength may explain the contrasting behavior between $v_{p,n}$ and $v_{p,p}$ upon drying. During drying, it was consistently observed that desiccation macro-crack solely formed parallel to bedding, suggesting that tensile stresses in excess of $\sigma_{t,n}$ were generated while $\sigma_{t,p}$ was not exceeded.

As mentioned above, $v_{p,p}$ showed no major variation in the range of suction tested in this study (i.e., 1.4 to 224.9 MPa). In the same range of suction, the Young's modulus and Poisson's ratio changed substantially from

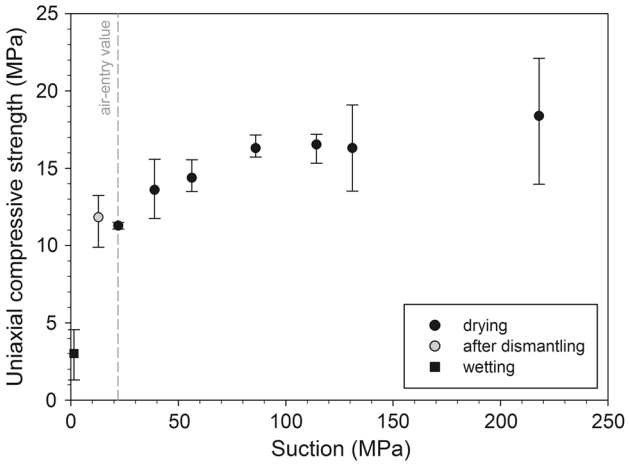

Fig. 16 Relationship between uniaxial compressive strength and suction. Mean value and data range for each applied suction are given

approximately 5 to 25 GPa, and 0.25 to 0.1, respectively (Figs. 12, 13). Assuming a linear-elastic material and a proportional relationship between dynamic and static elastic properties, there is evidence that the reason for the constant $v_{p,p}$ throughout the range of suction tested can be related to an opposing evolution of the Young's modulus and Poisson's ratio with increasing suction. The relationship between v_p and the dynamic elastic moduli is given by

$$v_p = \left[\frac{E}{\rho}\left(1 - \frac{2\upsilon^2}{1-\upsilon}\right)^{-1}\right]^{\frac{1}{2}} \quad (8)$$

From Eq. (8), it can be seen that for an increase in Young's modulus, the Poisson's ratio has to decrease to maintain a constant v_p. Even though the material tested in this study can be considered as transversal isotropic, and the relationship between static and elastic moduli is not known for this material, it is reasonable to assume that the independence between v_p and suction is associated with the disproportional trend in Young's modulus and Poisson's ratio and their opposing effect on p-wave velocity.

5.2 Strength and Stiffness Increase

Fredlund et al. (1995), Vanapalli et al. (1996) and Fredlund and Vanapalli (2002) analyzed shear strength variation of soils associated with variations in suction. They found that the increase in shear strength with increasing suction is linear up to a suction equal to the air-entry value. For suction beyond the air-entry value, the shear strength increase often becomes nonlinear depending on the soil type. For highly plastic clays, the increase in shear strength can be linear for a wide range of suction. When the suction approaches the suction at residual water content, the strength may remain constant or decrease. Based on their experimental findings and considerations on the effective

stress law for shear failure in unsaturated porous media, they demonstrated that variations in shear strength are associated with the net contributions of the effective normal stress and suction to the shear strength. The relation between soil shear strength and soil water retention characteristics is primarily based on the following equation, where changes in total stress and pore-water pressure are handled independently by two stress state variables:

$$\tau = c' + (\sigma_n - u_a)\tan\phi' + (u_a - u_w)\beta\tan\phi' \quad (9)$$

where c' is the effective cohesion, u_a is the pore-air pressure, ϕ' is the effective friction angle, u_w is the pore-water pressure and β represents the decrease in effective stress resistance as suction increases. The factor β equals 1 for saturated conditions and decreases with decreasing volumetric water content (Fredlund et al. 1995). Thus, the net contribution of capillary suction to shear strength decreases with decreasing volumetric water content (or wetted area between soil particles as suggested by Vanapalli et al. (1996)). At residual water content, this may cause a drop in shear strength. The above findings are consistent with observations in the present study: the tensile strength, the onset of dilatancy, the unconfined compressive strength and the stiffness increased almost linearly up to a suction of 56.6 MPa. For suction larger than 56.6 MPa, the scatter in the data points suggest only little variations in *CI*, *E*, *UCS* and $\sigma_{t,n}$, whereas $\sigma_{t,p}$ dropped significantly. Due to the scatter in the data, however, the onset of a nonlinear strength increase for suction beyond the air-entry value as suggested by Fredlund et al. (1995) could not be identified.

5.3 State-Dependent Strength Anisotropy

The comparison between the increase in $\sigma_{t,p}$ and $\sigma_{t,n}$ with an increase in suction suggest that $\sigma_{t,p}$ is considerably more affected by changes in suction than in $\sigma_{t,n}$. Similar tendencies can be found for the unconfined compressive strength on specimens loaded parallel and perpendicular to the bedding orientation. Amann et al. (2010) used both their own and published data to establish a relationship between water content and *UCS* of OPA specimens loaded perpendicular to bedding (Fig. 17). They found that in a range of water content between 8 and 5 %, the *UCS* increases with decreasing water content by a ratio of 5:1. Figure 17 also shows *UCS* data obtained in this study from specimens loaded parallel to bedding. The *UCS* increases with decreasing water content at a ratio of 1:1 in a range of water content between 7 and 1 %. These finding suggest a state-dependent strength anisotropy.

As shown in the previous sections, the desiccation damage evolves at high saturation (i.e., between 100 and 95 %), causing bedding parallel desiccation macro-cracks associated with a sharp drop in $v_{p,n}$. Desiccation cracks

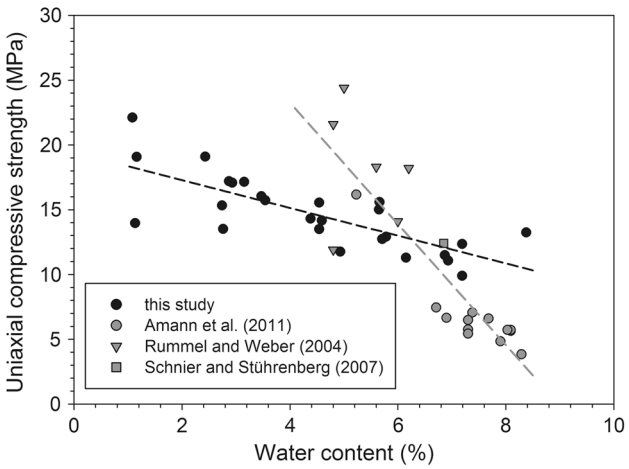

Fig. 17 Relationships between water content and *UCS* for specimens loaded parallel to bedding (*black*), and normal to bedding (*gray*)

parallel to bedding can affect $\sigma_{t,n}$, but do not or only marginally affect $\sigma_{t,p}$. However, desiccation cracking occurred at relatively high saturation or suction smaller than the air-entry value. For suction larger than the air-entry value, the data suggest no further damage accumulation (i.e., shrinkage limit). Thus, accumulated damage may not explain the dissimilar strength increase for suction greater than the air-entry suction.

State-dependent anisotropy in hydraulic conductivity of layered materials has been investigated by Yeh et al. (1985), Mualem (1984) and Green and Freyberg (1995). They consistently showed that the anisotropy in hydraulic conductivity increases with increasing suction. The reason for this increase is most probably related to the spatial variability in suction within a layered system, as illustrated in Fig. 18a (Green and Freyberg 1995). Due to the bedding fabric of OPA, it is likely that the mean applied suction is not uniformly distributed in the specimens (mainly due to variability in pore space distribution). Houben et al. (2013) found from detailed analyses that the REA for mineralogical composition and pore-size distribution is in the order of 100 × 100 μm^2. For smaller areas, considerable variations in pore-size distribution exist, suggesting that local variations in suction are to be anticipated. They also found that the majority of pores are aligned parallel to bedding. According to the results obtained in this study, these variations may cause stiffness and strength contrasts between zones of different pore-size distribution and may influence the effect of suction on strength and strength increase. Cracks in brittle rock types, such as OPA, tend to grow predominately sub-parallel to the maximum applied load (Amann et al. 2011, 2012). For a load applied parallel to bedding, cracks may grow along bedding layers with comparably low suction. If the load is applied normal to bedding growing fractures sub-parallel to the applied load

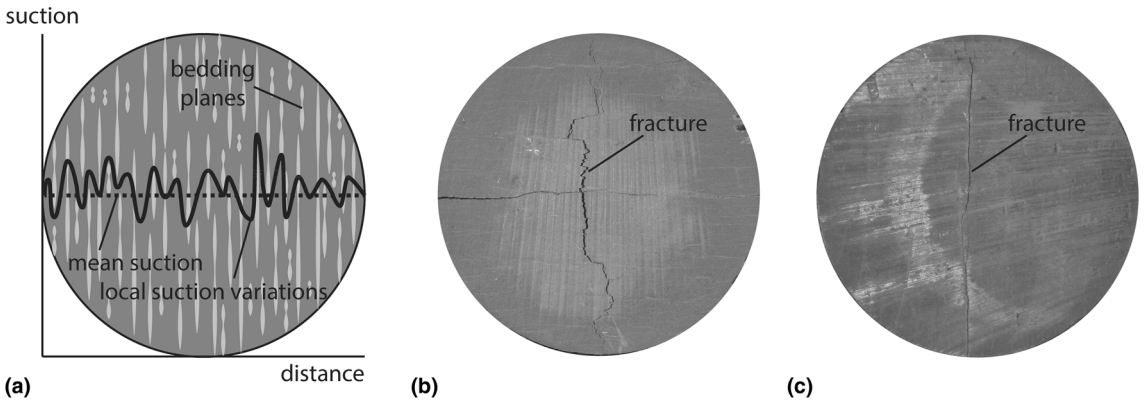

Fig. 18 Concept of local suction variation: **a** conceptual model, **b** photo of a Brazilian tensile strength specimen loaded normal to bedding with a stepped fracture, **c** photo of a specimen loaded parallel to bedding with a straight fracture (the *dipping lines* were created during cutting of the specimen)

direction may arrest at layers with higher suction and thus strength and stiffness (Amann et al. 2011, 2013a, b). The differences in crack propagation are illustrated in Fig. 18b, c for typical Brazilian tensile strength specimens loaded parallel and perpendicular to bedding. For the latter, the tensile fracture shows a stepped trace, indicating that fracturing is affected by heterogeneities in strength or stiffness between different regions. This is in contrast to fractures that form for tests with the load applied parallel to bedding, where typically a single fracture parallel to bedding formed.

6 Conclusions

A series of tests on specimens in equilibrium with various humidity (i.e., calculated suction between 1.4 and 224.9 MPa) were used to investigate strength (unconfined compressive strength, onset of dilatancy, Brazilian tensile strength), elastic properties (Young's modulus and Poisson's ratio) and ultrasonic p-wave velocity variations of Opalinus Clay. The results show that the p-wave velocity normal to bedding drops sharply upon desaturation until suction approached the air-entry value. The sharp decrease is associated with desiccation cracks solely oriented parallel to bedding. The p-wave velocity parallel to bedding remained constant in the range of suction investigated in this study. The constant $v_{p,p}$ with increasing suction might be associated with the disproportional decrease in the Poisson's ratio and E, and its opposing effect on p-wave velocity.

An almost linear increase in UCS, σ_t, CI and E with increasing suction was observed up to a suction value of 56.6 MPa. For suction exceeding 56.6 MPa, a relatively constant strength and stiffness was observed (except for $\sigma_{t,p}$ which showed a significant drop). The strength/stiffness increase is most probably associated with the net contribution of suction to strength, which decreases with decreasing volumetric water content nonlinearly, following the water retention characteristics.

The rate of increase in σ_t and UCS with increasing suction is different depending on the rock anisotropy. Both σ_t parallel to bedding and UCS obtained from specimens loaded normal to bedding increase with a considerably larger rate when suction increases. Reasons for the different rates in strength increase are most probably associated with local variations in suction (i.e., local suction) as a consequence of the bedded nature of Opalinus Clay with various zones of contrasting pore-size distribution. These variations in pore size may influence the effect of suction on strength when the applied load is parallel to bedding and crack growth is predominately along bedding layers with comparably low suction.

Acknowledgments This study was funded by the Swiss Federal Nuclear Waste Inspectorate. We are grateful to Dr. Keith Evans, Dr. Nicola Tisato, Dr. Benoît Valley (all Swiss Federal Institute of Technology, Zurich) and Dr. Paul Bossart (Swisstopo) for the fruitful discussions during execution and interpretation of the test results.

References

Amann F, Button EA, Blümel M, Thoeny R (2010) Insight into the mechanical behavior of Opalinus Clay. In: Zhao J, Labiouse V, Dudt J-P, Mathier J-F (eds) Rock mechanics and environmental engineering. Paper presented at European rock mechanics symposium 2010, Lausanne, Switzerland. Taylor & Francis Group, London, pp 759–762. ISBN 978-0-415-58654-2

Amann F, Button EA, Evans KF, Gischig VS, Blümel M (2011) Experimental study of the brittle behavior of clay shale in short-term unconfined compression. Rock Mech Rock Eng 44(4): 415–430

Amann F, Kaiser PK, Button EA (2012) Experimental study of the brittle behavior of clay shale in rapid confined compression. Rock Mech Rock Eng 44(1):21–33

Amann F, Ündül Ö, Kaiser PK (2013a) Crack initiation and crack propagation in heterogeneous sulfate-rich clay rocks. Rock Mech Rock Eng. doi:10.1007/s00603-013-0495-3

Amann F, Ündül Ö, Kaiser PK (2013b) Brittle failure processes in veined clay rock with large strength contrasts between vein and matrix. Paper presented at the 47th US rock mechanics/geomechanics symposium, San Francisco, CA, USA

Birle EM (2012) Geohydraulische Eigenschaften verdichteter Tone unter besonderer Berücksichtigung des ungesättigten Zustandes. PhD Thesis, Technischen Universität München

Bock H (2008) RA experiment: updated review of the rock mechanics properties of the Opalinus Clay of the Mont Terri URL based on laboratory and field testing. Unpublished Mont Terri Technical Report TR 2008-04

Brace WF, Paulding BR, Scholz C (1966) Dilatancy in fracture of crystalline rocks. J Geophys Res 71(16):3939–3953

Chae J, Kim B, Park S-W, Kato S (2010) Effect of suction on unconfined compressive strength in partly saturated soils. KSCE J Civ Eng 14(3):281–290

Corte A, Higashi A (1960) Experimental research on desiccation cracks in soil. U.S. Army, Ice and Permafrost Research Establishment, Hanover, N.H. Research Report 66

Cui YJ, Delage P (1996) Yielding and plastic behavior of an unsaturated compacted silt. Géotechnique 46(2):291–311

Dyke CG, Dobereiner L (1991) Evaluating the strength and deformability of sandstones. Q J Eng Geol Hydrogeol 24:123–134

Escario V, Jucá JFT, Coppe MS (1989) Strength and deformation of partly saturated soils. In: Proceedings of the twelfth international conference on soil mechanics and foundation engineering, vol 1, pp 43–46

Ferrari A, Laloui L (2013) Advances in the testing of the hydro-mechanical behaviour of shales. In: Laloui L, Ferrari A (eds) Multiphysical testing of soils and shales. Springer series in geomechanics and geoengineering, pp 57–68

Feuerharmel C, Pereira A, Gehling WYY, Bica AVD (2006) Determination of the shear strength parameters of two unsaturated colluvium soils using the direct shear test. In: Proceedings of the fourth international conference on unsaturated soils, pp 1181–1190

Fredlund DG, Vanapalli SK (2002) Shear strength of unsaturated soils. Agronomy Soil Testing Manual, Agronomy Society of America, Madison, pp 329–361

Fredlund DG, Morgenstern HR, Widger RA (1978) The shear strength of partly saturated soils. Géotechnique 36(3):453–456

Fredlund DG, Rahardjo H, Gan JK-M (1987) Non-linearity of strength envelope for unsaturated soils. In: Proceedings of the 6th international conference on expansive soils, New Delhi, India, 1–4 Dec 1987, pp 49–54

Fredlund DG, Xing A, Fredlund MD, Barbour SL (1995) The relationship of the unsaturated soil shear strength function to soil-water characteristic curve. Can Geotech J 32:440–448

Green TR, Freyberg DL (1995) State-dependent anisotropy: comparison of quasi-analytical solutions with stochastic results for steady gravity drainage. Water Resour Res 31(9):2201–2211

Houben ME, Desbois G, Urai JL (2013) Pore morphology and distribution in the Shaly facies of Opalinus Clay (Mont Terri, Switzerland): insight from representative 2D BIM-SEM investigations on mm to nm scale. Appl Clay Sci 71:82–97

Hsu SC, Neson P (1993) Characterization of cretaceous clay-shales in North America. Geotech Eng Hard Soils Soft Rocks 1:139–146

ISRM (1978) Suggested methods for determining tensile strength of rock materials. Int J Rock Mech Min Sci Geomech Abstr 15:99–103

ISRM (1979a) Suggested methods for determining the uniaxial compressive strength and deformability of rock materials. Int J Rock Mech Min Sci Geomech Abstr 16(2):135–140

ISRM (1979b) Suggested methods for determining water content, porosity, density, absorption and related properties and swelling and slake-durability index properties. Int J Rock Mech Min Sci Geomech Abstr 16(2):141–156

Klinkenberg M, Kaufhold S, Dohrmann R, Siegesmund S (2009) Influence of carbonate microfabrics on the failure strength of claystones. Eng Geol 107:42–54

Lajtai EZ (1974) Brittle fracture in compression. Int J Fract 10(4):525–536

Lashkaripour GR, Passaris EK (1995) Correlations between index parameters and mechanical properties of shales. In: Proceedings of the 8th international congress on rock mechanics, Tokyo, vol 1, pp 257–261

Mualem Y (1984) Anisotropy of unsaturated soil. Soil Sci Soc Am J 48:505–509

Nam S, Gutierrez M, Diplas P, Petrie J (2011) Determination of the shear strength of unsaturated soils using the multistage direct shear test. Eng Geol 122:272–280

Papamichos E, Brignoli M, Santarelli FJ (1997) An experimental and theoretical study of a partially saturated collapsible rock. Mech Cohes Frict Mater 2:251–278

Peron H, Hueckel T, Laloui L, Hu LB (2009) Fundamentals of desiccation cracking of fine-grained soils: experimental characterization and mechanisms identification. Can Geotech J 46:1177–1201

Peterson RFW(1988) Interpretation of triaxial compression test results on partially saturated soils. In: Advanced triaxial testing of soil and rock, ASTM STP 977. American Society for Testing and Materials, Philadelphia, pp 512–538

Rahardjo H, Lim TT, Chang MF, Fredlund DG (1995) Shear-strength characteristics of a residual soil. Can Geotech J 32:60–77

Ramos Da Silva M, Schroeder C, Verbrugge J-C (2008) Unsaturated rock mechanics applied to a low porosity shale. Eng Geol 97:42–52

Rummel F, Weber U (2004) RA experiment: rock mechanical testing and characterization on drillcores of boreholes BRA-1 and BRA-2. Unpublished Mont Terri Technical Note TN 2004-38

Schmitt L, Forsans T, Santarelli FJ (1994) Shale testing and capillary phenomena. Int J Rock Mech Min Sci Geomech Abstr 31(5):411–427

Schnellmann R, Rahardjo H, Schneider HR (2013) Unsaturated shear strength of a silty sand. Eng Geol 162:88–96

Schnier H, Stührenberg D (2007) LT experiment: strength tests on cylindrical specimens, documentation and evaluation. Unpublished Mont Terri Technical Report TR 2003-04

Thury M, Bossart P (1999) Mont Terri rock laboratory, results of the hydrogeological, geochemical and geotechnical experiments performed in 1996 and 1997, Landeshydrologie und -geologie, Geologischer Bericht Nr. 23

Valès F, Minh DN, Gharbi H, Rejeb A (2004) Experimental study of the influence of the degree of saturation on physical and mechanical properties in Tournemire shale (France). Appl Clay Sci 26:197–207

Van Genuchten MT (1980) A closed-form equation for predicting the hydraulic conductivity of unsaturated soils. Soil Sci Soc Am J 44:892–898

Vanapalli SK, Fredlund DG, Pufahl DE, Clifton AW (1996) Model for the prediction of shear strength with respect to soil suction. Can Geotech J 33:379–392

West G (1994) Effect of suction on the strength of rock. Q J Eng Geol Hydrogeol 27:51–56

Wild KM (2010) Charakterisierung des Verhaltens von Opalinuston unter Zugbeanspruchung. Unpublished Bachelor Thesis, ETH Zurich

Yeh TCJ, Gelhar LW, Gutjahr AL (1985) Stochastic analysis of unsaturated flow in heterogeneous soil, 2, statistically anisotropic media with variable α. Water Resour Res 21(4):457–464